Three-dimensional induced pluripotent stem-cell models of human brain angiogenesis

Peter Searson (searson@jhu.edu)
Johns Hopkins University https://orcid.org/0000-0002-5417-0828
Raleigh M. Linville
Johns Hopkins University Department of Biomedical Engineering
Diego Arevalo
Johns Hopkins University Department of Biomedical Engineering
Joanna C. Maressa
Johns Hopkins University Whiting School of Engineering
Nan Zhao
Johns Hopkins University Whiting School of Engineering

Research

Keywords: brain angiogenesis, induced pluripotent stem cells, brain microvascular endothelial cells, microvascular tissue engineering, blood-brain barrier, brain capillaries

Posted Date: December 10th, 2019

DOI: https://doi.org/10.21203/rs.2.18502/v1

Abstract

Background: During brain development, chemical cues released by developing neurons, cellular signaling with pericytes, and mechanical cues within the brain extracellular matrix (ECM) promotes angiogenesis occurs of brain microvascular endothelial cells (BMECs). During brain disease, angiogenesis can also occur due to pathological chemical, cellular, and mechanical signaling. Existing in vitro and in vivo models of brain angiogenesis have key limitations.

Methods: Here, we develop a high-throughput in vitro BBB bead assay of brain angiogenesis utilizing 150 μm diameter beads coated with induced pluripotent stem-cell (iPSC)-derived human BMECs (dhBMECs). After embedding the beads within a 3D matrix, we introduce various chemical cues and extracellular matrix components to explore their effects on angiogenic behavior. Based on the results from the bead assay, we generate a multi-scale model of the human cerebrovasculature within perfusable three-dimensional tissue-engineered blood-brain barrier (BBB) microvessels.

Results: A sprouting phenotype is optimized in confluent monolayers of dhBMECs using chemical treatment with vascular endothelial growth factor (VEGF) and wnt ligands, and the inclusion of pro-angiogenic ECM components. As a proof-of-principle that the bead angiogenesis assay can be applied to study pathological angiogenesis, we show that oxidative stress can exert concentration-dependent effects on angiogenesis. Finally, we demonstrate the formation of a hierarchical microvascular model of the human blood-brain barrier displaying key structural hallmarks.

Conclusions: We develop two in vitro models of brain angiogenesis: the BBB bead assay and the tissue-engineered BBB microvessel model. These platforms provide a tool kit for studies of physiological and pathological brain angiogenesis, with key advantages over existing two-dimensional models.

Background

Brain angiogenesis is a multistage process by which new capillaries sprout from existing blood vessels. The culmination of brain angiogenesis during development results in a 600 km network of capillaries forming the blood-brain barrier (BBB) [1]. Brain microvascular endothelial cells (BMECs), which form the interface between the vascular system and the brain parenchyma, regulate transport into the brain via expression of tight junctions (TJs), efflux pumps, and nutrient transporters [2, 3]. The ability to study brain angiogenesis in vitro has been limited by a lack of 3D models and an appropriate source of brain microvascular endothelial cells. Consequently, previous studies have relied on two-dimensional assays such as the Matrigel tube assay or cord-forming assays, or utilize primary / immortalized cells, which display an incomplete BBB phenotype [4, 5].

To enable imaging of angiogenesis in 3D, we have adapted the fibrin bead angiogenesis assay [6], forming a confluent monolayer of iPSC-derived brain microvascular endothelial cells (dhBMECs) on microbeads (BBB beads). The beads are then embedded in collagen I hydrogels, which mimic the native stiffness of brain parenchyma [7]. We then explore how changes in the chemical and extracellular matrix

microenvironment influence in vitro brain angiogenesis. We report on the influence of pro-angiogenic cues including vascular endothelial growth factor (VEGF) [8], wnt7a/b [9], and basement membrane [10]. In addition, to mimic pathological angiogenesis in response to oxidative stress, we report on the dose-dependent effects of hydrogen peroxide.

dhBMECs have emerged as an attractive cell source for BBB models as: (1) species differences mean that animal models do not always recapitulate human disease [11, 12], (2) reliable and diverse protocols have been developed to differentiate BMECs [13–15], and (3) patient-specific and CRISPR gene-edited iPSCs are available for controlled studies on how genetic mutations impact cell phenotype [16–18]. Additionally, dhBMECs recapitulate key aspects of BBB phenotype including high transendothelial electrical resistance, restriction of paracellular permeability, and efflux activity [3]. Primary and immortalized BMECs are often deficient in these characteristics and are not easily scalable for studies with isogenic or patient-specific models [19].

We also apply our results from the BBB bead angiogenesis assay to improve design of tissue-engineered hierarchical BBB models. Existing 3D models of brain angiogenesis based on self-organization approaches [20–22] fail to recapitulate the hierarchy of the human BBB, consisting of capillaries fed by an input arteriole and output venule. Engineering hierarchal microvascular models is limited by the spatial and temporal resolution of current techniques [22–25]. Our lab has demonstrated a hybrid approach relying on both templating and angiogenesis to form hierarchical microvascular networks using human umbilical vein endothelial cells (HUVECs) [26]. Here, after formation of microvessels resembling post-capillary venules (PCVs) by seeding dhBMECs into channels patterned within ECM [27], we apply optimized angiogenic factors to promote sprouting and anastomosis between adjacent microvessel to recapitulate a key aspect of human BBB function, low solute permeability. Our three-dimensional models provide a diverse toolbox for studies of developmental and pathological angiogenesis.

Methods

Cell culture

Brain microvascular endothelial cells (BMECs) were differentiated from hiPSCs similar to published protocols [15, 27]. The WTC iPSC line [28] with RFP-tagged plasma membrane (Allen Cell Institute) was used to facilitate live-cell monitoring of angiogenesis. WTC iPSCs were plated at 10,000 cells cm^{-2} on Matrigel-coated plates and grown for two days in mTESR1 (StemCell Technologies) to approximately 25% confluency, with 10 μM ROCK inhibitor Y27632 (RI; ATCC) supplemented for the initial 24 hours. Subsequent six-day treatment with unconditioned media without bFGF (UM/F-): DMEM/F12 (Life Technologies) supplemented with 20% knockout serum replacement (Life Technologies), 1% non-essential amino acids (Life Technologies), 0.5% GlutaMAX (Life Technologies) and 0.836 μM beta-mercaptoethanol (Life Technologies), and two-day treatment with RA media: human endothelial cell serum-free media (Life Technologies) supplemented with 1% human platelet poor derived serum (Sigma), 2 ng mL^{-1} bFGF (R&D Systems), and 10 μM all-trans retinoic acid (Sigma) produces dhBMECs.

Differentiations were conducted over a ten-passage window on six-well plates using media volumes of 1 mL and daily media switches. Transendothelial electrical resistance (TEER) measurements were used to confirm the quality of differentiations as previously reported [15]; the average TEER for WTC-RFP cells after 48 hours was ~ 2,500 Ω cm^2.

VeraVec HUVEC-TURBO-GFP cells (HUVECs; Angiocrine Bioscience) were used as a non-brain specific endothelial cell control. HUVECs were grown in “HUVEC media”: MCDB 131 (Caisson) supplemented with 10% fetal bovine serum (Sigma), 1% pen-strep-glut (Thermo Fisher), 1 µg mL^{-1} hydrocortisone (Sigma), 10 µg mL^{-1} heparin (Sigma), 25 µg mL^{-1} endothelial cell growth supplement (Thermo Fisher), and 0.2 mM ascorbic acid 2-phosphate (Sigma). HUVECs were used until passage 7 and routinely passed using TrypLE Express (Life Technologies).

Forming endothelial monolayers on microbeads

Assay protocols were adapted from those developed for primary endothelial cells [6]. 150 µm diameter Cytodex™ 3 microcarrier beads (GE Healthcare) were prepared according to manufacturer recommendations. Beads were coated overnight with 50 µg mL^{-1} human placental collagen IV (Sigma) and 25 µg mL^{-1} fibronectin from human plasma (Sigma). dhBMECs were singularized using 30 minute StemPro accutase (ThermoFisher) treatment and incubated at a ratio of 1000:1 (dhBMECs:beads) for two hours under gentle agitation every 30 minutes. “Bead seeding media” was comprised of human endothelial cell serum-free media (Life Technologies) supplemented with 1% human platelet poor derived serum (Sigma), 1% Penicillin Streptomycin (Thermo Fisher), 2 ng mL^{-1} bFGF (R&D Systems), 10 µM all-trans retinoic acid (Sigma), and 10 µM ROCK inhibitor Y27632 (RI). Inclusion of RI was required to enable cell adhesion, as previously found for collagen-based biomaterials [29]. After two hours, non-adherent dhBMECs were removed and beads were cultured for 24 hours on a shaker at 100 rpm in bead seeding media. To form HUVEC coated beads, identical protocols were used with the following differences: (1) incubation with cells for only one hour, (2) use of HUVEC media without supplementation with RI.

Immunocytochemistry

After 24 hours on a shaker (day 1), beads were fixed and stained to assess protein expression. Beads were rinsed with room-temperature phosphate-buffered saline (PBS; ThermoFisher) and then collected using brief centrifugation (30 seconds at 0.3 g). Beads were fixed using ice-cold methanol for 15 minutes, blocked for 30 minutes in PBS with 10% normal goat serum (Cell Signaling Technology) and 0.3% Triton X-100 (Millipore Sigma), and then treated with primary antibodies diluted in blocking buffer overnight at 4 ˚C (see Supplementary Table S1 for details). After washing with PBS three times, cells were treated with 1:200 Alexa Flour-488 or Alexa Flour-647 secondary antibodies (Life Technologies) diluted in blocking buffer for 45 minutes at room temperature. To physically constrain beads for confocal imaging and to stain cell nuclei, beads were loaded onto eight-chambered borosilicate cover glass wells with Fluoromount-G with DAPI (Invitrogen). Confocal images were acquired at 40x magnification on a swept field confocal microscope system (Prairie Technologies) with illumination provided by an MLC 400 monolithic laser combiner (Keysight Technologies). As a negative control, beads were not exposed to

primary antibodies to determine signal due to non-specific secondary antibody binding. To conduct immunocytochemistry of microvessels, antibodies and buffers were perfused through microvessel lumens with identical incubation times.

Permeability assay

Beads were suspended in 200 μM Lucifer yellow (CH dilithium salt; LY) (Sigma) to confirm barrier formation. After three hours, confocal images were acquired at the bead midplane to determine accumulation of LY from the fluorescence within beads. Three conditions were tested: (1) blank beads without LY, (2) blank beads with LY, and (3) dhBMEC beads with LY. A circular region of interest (ROI) within beads was used to compare normalized fluorescence intensity across conditions.

Bead angiogenesis assay

On day 1 (24 hours after seeding dhBMECs), beads were suspended into hydrogels at ~ 100 beads mL^{-1} and gelled in a 250 μL volume within eight-chambered borosilicate cover glass wells (Lab Tek). Hydrogels were comprised of 6 mg mL^{-1} neutralized rat tail type I collagen (Corning). After 30 minutes of gelation, cell culture media was added on top of hydrogel and replenished daily. Both cell culture media and ECM conditions were toggled to optimize angiogenic growth. Basal media consisted of human endothelial cell serum-free media (Life Technologies) supplemented with 1% human platelet poor derived serum (Sigma) and 1% Penicillin Streptomycin (Thermo Fisher). Basal media was further supplemented with bFGF (R&D Systems), recombinant human Wnt-7a (Wnt7a; Fisher Scientific), and recombinant Human VEGF-165 (VEGF; Biolegend). In some experiments, hydrogels were supplemented with additional ECM components, including 1.5 mg mL^{-1} growth factor reduced Matrigel (Corning), 1.5 mg mL^{-1} fibrin, and 0.5 mg mL^{-1} fibronectin from human plasma. Fibrin composite hydrogels were formed by combining 2 U mL^{-1} thrombin from bovine plasma (Sigma) with 6 mg mL^{-1} neutralized rat tail type I collagen (Corning), before addition of 1.5 mg mL^{-1} fibrinogen from bovine plasma (Sigma). Across all experiments, media was replenished daily (250 μL volume).

Imaging and analysis

Phase contrast and epifluorescence images (Texas Red filter) of beads were acquired on an inverted microscope (Nikon Eclipse TiE) at 10x magnification. For each experimental condition, ten images (technical replicates) of individual beads were collected at day 2, 4 and 6 after embedding in hydrogels. Beads whose endothelium grew along the glass-collagen interface were excluded from analysis. Angiogenic sprouts were defined as perpendicular protrusions from beads, with length greater than thickness. Three measures were calculated in ImageJ (NIH): (1) Angiogenic percentage (%), defined as the percentage of beads that display angiogenic sprouts, (2) sprout density (# $bead^{-1}$), and (3) maximum sprout length (μm).

Modeling oxidative stress

Hydrogen peroxide (H_2O_2; Sigma) was prepared in water and then supplemented in media to final concentrations of 1 mM and 10 μM. Vehicle treatment consisted of 1% water. H_2O_2 was added after embedding beads in hydrogels and was included in daily media switches. All oxidative stress experiments were conducted in 6 mg mL^{-1} rat tail type I collagen and 1.5 mg mL^{-1} Matrigel, treated with basal media for 6 days.

Microvessel fabrication

Three-dimensional BBB microvessels were fabricated as previously reported [27]. Briefly, 1 cm (length) x 1.75 mm (width) x 1 mm (height) channels were cast in polydimethylsiloxane (PDMS; Dow Corning) using an aluminum mold. Neutralized 6 mg mL^{-1} rat tail type I collagen supplemented with 1.5 mg mL^{-1} Matrigel was gelled surrounding a template 150 μm diameter super-elastic nitinol wire (Malin Co.). After 30 minutes at 37 ˚C, template wires were removed to leave behind a channel that was subsequently seeded with singularized dhBMECs. Microvessels were perfused under ~ 2 dyne cm^{-2} shear stress using fluid reservoirs as previously reported [7]. For the first 24 hours, “bead seeding medium” was perfused through channels to promote microvessel formation. Then, experimental media were perfused for 6 days.

Hierarchical model

A hierarchical microvascular model was fabricated based on a previously reported model using HUVECs [26]. Two template 150 μm diameter super-elastic nitinol wires were suspended with a separation distance (d) of approximately 200 μm. Microvessels were perfused at 2 dyne cm^{-2} shear stress. All hierarchical models were generated in 6 mg mL^{-1} rat tail type I collagen and 1.5 mg mL^{-1} Matrigel, perfused with basal media + 20 ng mL^{-1} bFGF for 5 days. To assess barrier function, 2 μM 500 kDa dextran (Thermo Fisher) was perfused through microvessels for thirty minutes before, during, and after anastomosis. Phase contrast and fluorescence images were acquired every two minutes, as previously reported [7]. ImageJ was used to plot fluorescence intensity over time, where permeability is calculated as $(r/2)(1/\Delta I)(dI/dt)0$, where r is the microvessel radius, ΔI is the jump in total fluorescence intensity upon luminal filling, and $(dI/dt)_0$ is the rate of increase in total fluorescent intensity over one hour [27, 30].

Statistical Analysis

Statistical testing was performed using Prism ver. 8 (GraphPad). Measures are reported as mean ± standard error of the mean (SEM). A one-way analysis of variance (ANOVA) test was used for comparison of three or more groups. Reported p-values were multiplicity adjusted using a Tukey test. Differences were considered statistically significant for $p < 0.05$, with the following thresholds: * $p < 0.05$, ** $p < 0.01$, *** $p < 0.001$.

Results

Fabrication of a three-dimensional of brain angiogenesis

To assess the angiogenic potential of iPSC-derived brain microvascular endothelial cells (dhBMECs), we adapted the bead angiogenesis assay [6]. dhBMECs were differentiated from the WTC iPSC line with a fluorescently-tagged plasma membrane (Fig. 1a, b). 150 μm diameter beads were coated with extracellular matrix (ECM) proteins collagen IV and fibronectin, and then incubated with dhBMECs for 2 hours to achieve a uniform coating (Fig. 1c, d). Beads were cultured for 24 hours to enable the formation of a confluent monolayer of dhBMECs (BBB beads). The beads were then embedded within extracellular matrix (ECM) to study chemical and physical cues that guide angiogenesis. An entire six-well plate of dhBMECs is sufficient for coating ~ 12,000 beads, demonstrating the scalability of our approach.

BBB beads display expression of critical BBB and endothelial markers, including claudin-5, occludin, glucose transporter 1 (GLUT1), p-glycoprotein (Pgp), and CD31 (Fig. 2a). Protein expression of BBB markers was unique to dhBMECs, while the endothelial marker (CD31) was also expressed by human umbilical vein endothelial cells (HUVECs) (Supp. Figure 1). Additionally, BBB beads express the critical angiogenic ligand receptors fibroblast growth factor receptor 2 (FGFR2), vascular endothelial growth factor receptor 2 (VEGFR2), and G protein-coupled receptor 124 (GPR124) (Fig. 2b). BBB beads were incubated in Lucifer yellow (LY) for 3 hours to confirm formation of a functional barrier (Fig. 2c). Three conditions were tested: (1) blank beads without LY, (2) blank beads with LY, and (3) beads with dhBMEC monolayers with LY. The core of the beads is comprised of a permeable dextran polymer and hence beads without a dhBMEC monolayer showed high fluorescence intensity after three hours incubation with LY. In contrast, beads with a dhBMEC monolayer significantly restricted accumulation of solutes within the core ($p < 0.001$) (Fig. 2d-e). These results suggest that beads coated with dhBMECs display a key phenotypic property of the human BBB.

Influence of chemical factors

To assess the influence of pro-angiogenic factors, we incubated BBB beads in three media conditions: (1) basal media, (2) basal media + 20 ng mL^{-1} bFGF, and (3) basal media + 20 ng mL^{-1} bFGF + 50 ng mL^{-1} VEGF + 50 ng mL^{-1} wnt7a. Across these conditions, the BBB beads were embedded within 6 mg mL^{-1} collagen I hydrogels. In the absence growth factors, angiogenic behavior was not widely observed (Fig. 3a): after six days, only 10% of beads displayed visible sprouts (Fig. 3b). In the presence of bFGF alone, some angiogenic behavior was observed. The angiogenic fraction and maximum sprout lengths were increased compared to beads cultured in the absence of bFGF ($p = 0.026$ and $p = 0.013$, respectively), while sprout density was not statistically different ($p = 0.097$) (Fig. 3b-d). The addition of VEGF and wnt7a produced on average higher angiogenic phenotype (Fig. 3a), which was increased compared to basal conditions ($p = 0.004$, 0.012, and 0.018, respectively), but not statistically significant compared to bFGF exposure alone (Fig. 3b-d). The average sprout length for BBB beads in VEGF and wnt7a increased linearly with time with a growth rate of approximately 20 μm day^{-1} (Fig. 3e). Confocal imaging of BBB beads cultured in VEGF and wnt7a show extensive networks of angiogenic sprouts and formation of lumen-like structures (Fig. 3f). Additionally, in comparison to HUVEC beads, sprouts on the BBB beads are shorter but have a higher density (Supp. Figure 2).

Influence of extracellular matrix components

To assess the role of matrix composition, we tested four ECM conditions: (1) 6 mg mL^{-1} collagen I, (2) 6 mg mL^{-1} collagen I + 1.5 mg mL^{-1} growth factor reduced Matrigel, (3) 6 mg mL^{-1} collagen I + fibronectin, and (4) 6 mg mL^{-1} collagen I + fibrin. Matrigel is predominately comprised of laminin, along with other ECM components [31]. Across these conditions, beads were exposed to basal media + 20 ng mL^{-1} bFGF + 50 ng mL^{-1} VEGF + 50 ng mL^{-1} wnt7a. Changing ECM composition (without dramatically altering hydrogel biomechanics) had a less dramatic effect on angiogenic phenotype compared to soluble angiogenic factors: a similar sprouting morphology were observed across the conditions (Fig. 4a). The angiogenic fraction was similar across additions of ECM components and significant differences were not observed ($p > 0.05$ for all comparisons) (Fig. 4b). Matrigel supplementation led to increased sprout compared to fibronectin, suggesting that these two ECM conditions represent the most and least pro-angiogenic, respectively ($p = 0.03$) (Fig. 4c). Maximum sprout length was generally increased due to additions of ECM components, but was not significantly different ($p > 0.05$ for all comparisons) (Fig. 4d). For all subsequent experiments collagen I was supplemented with Matrigel to recapitulate angiogenic phenotype.

Modeling pathological angiogenesis

To model pathological brain angiogenesis, we exposed the BBB beads to high and low concentrations of hydrogen peroxide (H_2O_2) in the absence of external growth factor stimuli. After two days exposure to 10 μM H_2O_2, the formation of sprouts into the ECM highlights an increased angiogenic phenotype (Fig. 5a). The sprout density was significantly increased compared to vehicle treatment ($p = 0.047$) (Fig. 5b). Interestingly, the pro-angiogenic effects of 10 μM H_2O_2 were not maintained over time as by day 6 angiogenic behavior was lost, while vehicle treatment displays minor angiogenic behavior (Fig. 5c). This suggests that 10 μM H_2O_2 exerts a bimodal effect of angiogenic phenotype. Interestingly, the addition of 100-fold higher H_2O_2 (1 mM) abrogates angiogenic behavior on much shorter time scales (no sprouts are observed) (Fig. 5a-c).

Perfusable microvessel models of brain angiogenesis

Next, we tested the role of chemical cues for in vitro dhBMEC angiogenesis within a tissue-engineered perfusable microvessel model. These experiments mimic techniques previously demonstrated to study angiogenesis from an existing three-dimensional microvessel [26, 32, 33]. Microvessels are formed in 150 μm diameter channels within 6 mg mL^{-1} type I collagen supplemented with 1.5 mg mL^{-1} Matrigel (Fig. 6a, b). Channels are seeded with dhBMECs, which under continual ~ 2 dyne cm^{-2} perfusion, assemble into BBB microvessels as previously reported [27]. After microvessel formation, we applied media conditions as tested in Fig. 3 to observe angiogenic behavior (Fig. 6c).

Under perfusion with basal media, angiogenic behavior is not widely observed and the microvessel structure remains stable over six days (Fig. 6d). Supplementation with bFGF results in early sprouts within two days, which continue to grow in length and branching complexity (Fig. 6d). Supplementation with bFGF, VEGF, and wnt7a resulted in an increased density of sprouts along microvessels after two

days, and chaotic sprouting behavior by six days (Fig. 6d). Both growth factor supplementation regimes were associated with loss of microvessel perfusion after 5–6 days due to overgrowth and constriction of microvessel lumens (data not shown). Based on these results we chose to further explore bFGF supplementation over four days to promote formation of organized microvascular lumens.

Hierarchical model of the human blood-brain barrier

Lastly, we sought to engineer a hierarchical model of the human brain microvasculature by promoting sprouting between adjacent BBB microvessels. This technique has previously been demonstrated using human umbilical vein endothelial cells (HUVECs) [26]. We patterned adjacent 150 μm diameter channels within 6 mg mL^{-1} type I collagen supplemented with 1.5 mg mL^{-1} Matrigel separated by 200 μm (Fig. 7a, b). After microvessel formation, microvessels were perfused at ~ 2 dyne cm^{-2} with basal media + 20 ng mL^{-1} bFGF (Fig. 7c). Continual perfusion over three days resulted in anastomosis of capillary sprouts (Fig. 7d).

Discussion

Factors that regulate in vitro brain angiogenesis

The formation of brain capillaries during development occurs through the convergence of multiple signaling pathways [2, 34]. Vascular endothelial growth factor (VEGF) released by the developing neural tube initiates formation of the perineural vascular plexus (PNVP) via vasculogenesis. From the PNVP, BMECs invade the brain parenchyma via angiogenesis driven by chemical cues released by developing neurons (e.g. wnt7a/b) and mechanical interactions with the brain parenchyma [2, 34]. The culmination of brain angiogenesis during development results in a hierarchical BBB with profound heterogeneity in structure and phenotype [35–37]. However, after development, angiogenesis is generally restricted to pathological conditions which alter BBB structure and phenotype [37–39]. Here we develop an in vitro model of brain angiogenesis using iPSC-derived BMECs (dhBMECs) to study developmental and pathological angiogenesis. We explore multiple factors that alter angiogenic phenotype of brain microvascular endothelial cells, including growth factors, ECM composition, and oxidative stress.

Critical chemical cues implicated in developmental brain angiogenesis include vascular endothelial growth factor (VEGF) [8] and wnt7a/b (WNT) [9]. WNT signaling is specifically required for brain angiogenesis and is harnessed during differentiation of hiPSC-derived BMECs [13]. However, other growth factors, including basic fibroblast growth factor (bFGF), are also implicated in promoting brain angiogenesis [40, 41]. Here we find that all three growth factors are likely pro-angiogenic for dhBMECs. In previous studies of primary brain microvascular endothelial cells using a tube formation assay [42], hypoxia was found to increase VEGF expression but was insufficient to promote formation of new vessels. In contrast, we find that angiogenic factors are sufficient to promote angiogenesis of dhBMECs within a 3D microenvironment, supporting the development of more physiological angiogenesis models.

Additionally, ECM composition and stiffness are key regulators of angiogenesis [43–48]. Numerous studies have shown that increased ECM stiffness reduces angiogenesis, likely by limiting cell proliferation and migration [46–48]. Pro-angiogenic ECM proteins include collagen I, fibronectin, and laminin [43]. In studies specific to BMECs, fibronectin and laminin were shown to promote angiogenic and maturation phenotype, respectively [49]. The extracellular space in the brain is comprised of hyaluronic acid, lecticans, proteoglycan link proteins, and tenascins [50, 51]. However, as the human brain is highly cellular by volume, non-brain-specific ECM components are commonly used to mimic the physical properties of the brain [3, 52, 53]. For example, 3D BBB models commonly utilize non-brain ECM components including collagen I [27, 54–58] and fibrin [20–22, 59]. We previously characterized and compared the stiffness of collagen I hydrogels to native mouse brain, and showed that 6 mg mL^{-1} collagen is a reasonable proxy for brain stiffness [7]. Additionally, materials with stiffnesses much lower than native brain were not conducive to the formation of stable BBB microvessels [7]. Thus, we chose to only explore ECM materials with sufficient stiffness to form perfusable microvessel models, despite their absence within the brain parenchyma. We find that addition of growth factor-reduced Matrigel (primarily composed of laminin) to a collagen I matrix increased angiogenic phenotype.

Under homeostatic conditions angiogenesis is not prevalent in the adult brain; however, brain angiogenesis is associated with pathological conditions, including neurodegenerative disease, brain cancer, and stroke [37]. Production of reactive oxygen species (ROS) is associated with these conditions and may contribute to BBB disruption and pathological angiogenesis [60]. Reactive oxygen species promote angiogenesis via both VEGF-dependent and independent mechanisms [61]. Previous work utilizing primary rat BMECs found that H_2O_2 displays a concentration-dependent influence on angiogenic behavior: concentrations below 10 μM increased tube length using a Matrigel tube formation assay, while concentrations above 10 μM decreased tube length [5]. Here, the use of BBB beads provides spatial and temporal resolution to study the time-dependent effects of oxidative stress, which have previously been ignored. We find that H_2O_2 exerts a bimodal and concentration-dependent effect on brain angiogenesis.

Model advantages and limitations

2D models of brain angiogenesis (i.e. transwell assay or Matrigel tube forming assay) are unable to recapitulate the spatial dynamics of BMEC sprouting. Recently, 3D models of the brain microvasculature have been engineered via mimicry of vasculogenesis or angiogenesis using co-cultured primary ECs or BMECs, pericytes, and astrocytes [20–22]. Additionally, a microfluidic model of neurogenesis and angiogenesis was formed using co-cultured mesenchymal stem cells, primary BMECs, and neural stem cells, but was not tested for functional BBB properties [59]. The use of hiPSC-derived BMECs in models of brain angiogenesis has not yet been demonstrated. Here, we build the first iPSC-derived in vitro model of brain angiogenesis. This model supports controlled studies of microenvironmental cues and genetic mutations on angiogenesis, without confounding factors present in vivo. Additionally, previous models have utilized fibrin for creating brain microvascular networks via angiogenesis and vasculogenesis-like processes [20–22]. However, fibrin is not conducive with dhBMEC microvessel formation and is rapidly

degraded (Supp. Figure 3). Although neither collagen I nor fibrin is found in native brain ECM, collagen I densities used in this study are similar to the mechanical stiffness of native brain.

There are two main limitations to our model. (1) Brain angiogenesis in vivo occurs in the presence of complex cell-cell interactions, which are neglected in our model: BMECs interact with neurons, neural progenitor cells, pericytes, and glial progenitors during brain angiogenesis. As previously discussed, neurons and neural progenitor cells release critical chemical stimuli including wnt ligands and VEGF, which we introduce to promote sprouting in our model. Pericytes are an important cellular component of the neurovascular unit as they physically support new capillaries and are required for the formation of the BBB during development [62, 63]. Astrocytes are not critically involved in angiogenesis, as they are not present during initial brain vascularization; however, postnatally, they release ligands that maintain BBB integrity [64]. Lastly, radial glia cells guide spatial patterning of angiogenesis as a physical scaffold for endothelial cell migration [34, 65]. Recent reports of an isogenic multicellular iPSC-based BBB transwell assay provide the foundations for building more complex angiogenesis models [66]. Additionally, we previously incorporated iPSC-derived pericytes into a 3D microvessel BBB model, showing that they do not significantly alter barrier properties [67]. Future work is required to examine how iPSC-derived pericytes and other cells of the BBB may alter angiogenesis in vitro. (2) The stability of angiogenic vessels is not addressed: the adult cerebrovasculature is highly stable, with limited angiogenesis [37]. For example, over 30 days changes in capillary length, diameter or branching were not observed in the adult mouse somatosensory and motor cortex [68]. Thus, models of the cerebrovasculature should aim to mimic physiological structural and phenotypic stability. We previously explored the stability of BBB microvessels, finding that microvessels reach quiescence over several days (when rates of cell division match cell apoptosis) [27]. However, stability of microvessels formed via angiogenesis has not been addressed. As growth factor expression can display unique temporal and spatial expression patterns [8], transient administration or removal of growth factors may aid in generating stable microvessels. Future work will explore how removal of growth factors after angiogenesis occurs alters the structural and phenotypic stability of tissue-engineered cerebrovascular models. Additionally, many other stimuli influence the morphology of microvasculature in vitro, including flow and shear stress [45, 69], which could be harnessed to promote stability.

Engineering BBB hierarchy

To promote sprouting and anastomosis of capillaries between adjacent tissue-engineered microvessels we applied angiogenic factors which maximized growth rates. In previous work, capillary growth rates of ~ 40 μm day^{-1} were sufficient to anastomose adjacent HUVEC microvessels [26]. Here we observed more modest growth rates for dhBMECs (~ 20 μm day^{-1}). Previously it has been found that iPSC-derived endothelial cells exhibit reduced angiogenic potential compared to primary ECs (HUVECs), likely due to differences in MMP production [70]. Due to limitations with primary and immortalized BMEC sources we did not explore cell source-dependent angiogenic differences. Importantly, our hierarchical model allows probing of how BBB phenotype changes across the vascular tree. Recently, we demonstrated use of BBB

microvessels for studying hyperosmotic BBB disruption [71], but do not know if capillaries are more susceptibility to opening.

Conclusions

Existing in vitro models have generally failed to mimic brain angiogenesis or recapitulate physiological barrier function, hierarchy, and zonation of the human BBB. Here, we develop 3D in vitro stem cell-based models of brain angiogenesis, including a high-throughput BBB bead assay and perfusable microvessel model. These models have diverse applications in screening the influence of chemical, mechanical, cell genotype, and stress signals on brain angiogenesis.

Abbreviations

BBB: blood-brain barrier; BMECs: brain microvascular endothelial cells; hiPSCs: human induced pluripotent stem cells; dhBMECs: hiPSC-derived BMECs; ECM: extracellular matrix; VEGF: vascular endothelial growth factor.

Declarations

Acknowledgements

RML acknowledges a National Science Foundation Graduate Research Fellowship under Grant No. DGE1746891. The authors acknowledge the assistance of Gabrielle Grifno, Matt Sklar, and Alanna Farrell with cell culture and microfabrication.

Author contributions

RML and DA designed, conducted, and analyzed bead assay experiments. RML, JM, and NZ designed, conducted, and analyzed microvessel experiments. RML and PCS wrote the manuscript. All authors read and approved the final manuscript.

Funding

This work was supported by DTRA (HDTRA1-15-1-0046) and NIH (R01NS106008).

Availability of data and materials

The raw and processed data from this study are available from the corresponding author.

Ethics approval and consent to participate

Not applicable.

Consent for publication

Not applicable.

Competing interests

The authors declare no conflict of interest.

References

1. Zlokovic, B.V., *Neurovascular mechanisms of Alzheimer's neurodegeneration.* Trends Neurosci, 2005. **28**(4): p. 202-8.
2. Zhao, Z., et al., *Establishment and Dysfunction of the Blood-Brain Barrier.* Cell, 2015. **163**(5): p. 1064-78.
3. DeStefano, J.G., et al., *Benchmarking in vitro tissue-engineered blood-brain barrier models.* Fluids Barriers CNS, 2018. **15**(1): p. 32.
4. Nowak-Sliwinska, P., et al., *Consensus guidelines for the use and interpretation of angiogenesis assays.* Angiogenesis, 2018. **21**(3): p. 425-532.
5. Anasooya Shaji, C., et al., *The Tri-phasic Role of Hydrogen Peroxide in Blood-Brain Barrier Endothelial cells.* Sci Rep, 2019. **9**(1): p. 133.
6. Nakatsu, M.N. and C.C. Hughes, *An optimized three-dimensional in vitro model for the analysis of angiogenesis.* Methods Enzymol, 2008. **443**: p. 65-82.
7. Grifno, G.N., et al., *Tissue-engineered blood-brain barrier models via directed differentiation of human induced pluripotent stem cells.* Sci Rep, 2019. **9**(1): p. 13957.
8. Ogunshola, O.O., et al., *Neuronal VEGF expression correlates with angiogenesis in postnatal developing rat brain.* Brain Res Dev Brain Res, 2000. **119**(1): p. 139-53.
9. Daneman, R., et al., *Wnt/beta-catenin signaling is required for CNS, but not non-CNS, angiogenesis.* Proc Natl Acad Sci U S A, 2009. **106**(2): p. 641-6.
10. Thomsen, M.S., L.J. Routhe, and T. Moos, *The vascular basement membrane in the healthy and pathological brain.* J Cereb Blood Flow Metab, 2017. **37**(10): p. 3300-3317.
11. Watase, K. and H.Y. Zoghbi, *Modelling brain diseases in mice: the challenges of design and analysis.* Nat Rev Genet, 2003. **4**(4): p. 296-307.
12. O'Brown, N.M., S.J. Pfau, and C. Gu, *Bridging barriers: a comparative look at the blood-brain barrier across organisms.* Genes Dev, 2018. **32**(7-8): p. 466-478.
13. Lippmann, E.S., et al., *Derivation of blood-brain barrier endothelial cells from human pluripotent stem cells.* Nat Biotechnol, 2012. **30**(8): p. 783-91.
14. Qian, T., et al., *Directed differentiation of human pluripotent stem cells to blood-brain barrier endothelial cells.* Sci Adv, 2017. **3**(11): p. e1701679.
15. Katt, M.E., et al., *Human Brain Microvascular Endothelial Cells Derived from the BC1 iPS Cell Line Exhibit a Blood-Brain Barrier Phenotype.* PLoS One, 2016. **11**(4): p. e0152105.

16. Katt, M.E., et al., *The role of mutations associated with familial neurodegenerative disorders on blood-brain barrier function in an iPSC model.* Fluids Barriers CNS, 2019. **16**(1): p. 20.
17. Lim, R.G., et al., *Huntington's Disease iPSC-Derived Brain Microvascular Endothelial Cells Reveal WNT-Mediated Angiogenic and Blood-Brain Barrier Deficits.* Cell Rep, 2017. **19**(7): p. 1365-1377.
18. Vatine, G.D., et al., *Human iPSC-Derived Blood-Brain Barrier Chips Enable Disease Modeling and Personalized Medicine Applications.* Cell Stem Cell, 2019. **24**(6): p. 995-1005 e6.
19. Helms, H.C., et al., *In vitro models of the blood-brain barrier: An overview of commonly used brain endothelial cell culture models and guidelines for their use.* J Cereb Blood Flow Metab, 2016. **36**(5): p. 862-90.
20. Bang, S., et al., *A Low Permeability Microfluidic Blood-Brain Barrier Platform with Direct Contact between Perfusable Vascular Network and Astrocytes.* Sci Rep, 2017. **7**(1): p. 8083.
21. Campisi, M., et al., *3D self-organized microvascular model of the human blood-brain barrier with endothelial cells, pericytes and astrocytes.* Biomaterials, 2018. **180**: p. 117-129.
22. Lee, S., et al., *3D brain angiogenesis model to reconstitute functional human blood-brain barrier in vitro.* Biotechnol Bioeng, 2019.
23. Gold, K., A.K. Gaharwar, and A. Jain, *Emerging trends in multiscale modeling of vascular pathophysiology: Organ-on-a-chip and 3D printing.* Biomaterials, 2018.
24. Bogorad, M.I., et al., *Review: in vitro microvessel models.* Lab Chip, 2015. **15**(22): p. 4242-55.
25. Traore, M.A. and S.C. George, *Tissue Engineering the Vascular Tree.* Tissue Eng Part B Rev, 2017. **23**(6): p. 505-514.
26. Bogorad, M.I., et al., *Tissue-engineered 3D microvessel and capillary network models for the study of vascular phenomena.* Microcirculation, 2017. **24**(5).
27. Linville, R.M., et al., *Human iPSC-derived blood-brain barrier microvessels: validation of barrier function and endothelial cell behavior.* Biomaterials, 2019. **190-191**: p. 24-37.
28. Kreitzer, F.R., et al., *A robust method to derive functional neural crest cells from human pluripotent stem cells.* Am J Stem Cells, 2013. **2**(2): p. 119-31.
29. Katt, M.E., et al., *Functional brain-specific microvessels from iPSC-derived human brain microvascular endothelial cells: the role of matrix composition on monolayer formation.* Fluids Barriers CNS, 2018. **15**(1): p. 7.
30. Huxley, V.H., F.E. Curry, and R.H. Adamson, *Quantitative fluorescence microscopy on single capillaries: alpha-lactalbumin transport.* Am J Physiol, 1987. **252**(1 Pt 2): p. H188-97.
31. Hughes, C.S., L.M. Postovit, and G.A. Lajoie, *Matrigel: a complex protein mixture required for optimal growth of cell culture.* Proteomics, 2010. **10**(9): p. 1886-90.
32. Nguyen, D.H., et al., *Biomimetic model to reconstitute angiogenic sprouting morphogenesis in vitro.* Proc Natl Acad Sci U S A, 2013. **110**(17): p. 6712-7.
33. Pauty, J., et al., *A Vascular Endothelial Growth Factor-Dependent Sprouting Angiogenesis Assay Based on an In Vitro Human Blood Vessel Model for the Study of Anti-Angiogenic Drugs.*

EBioMedicine, 2018. **27**: p. 225-236.

34. Walchli, T., et al., *Wiring the Vascular Network with Neural Cues: A CNS Perspective.* Neuron, 2015. **87**(2): p. 271-96.
35. Noumbissi, M.E., B. Galasso, and M.F. Stins, *Brain vascular heterogeneity: implications for disease pathogenesis and design of in vitro blood-brain barrier models.* Fluids Barriers CNS, 2018. **15**(1): p. 12.
36. Vanlandewijck, M., et al., *A molecular atlas of cell types and zonation in the brain vasculature.* Nature, 2018. **554**(7693): p. 475-480.
37. Bogorad, M.I., et al., *Cerebrovascular plasticity: Processes that lead to changes in the architecture of brain microvessels.* J Cereb Blood Flow Metab, 2019. **39**(8): p. 1413-1432.
38. Rigau, V., et al., *Angiogenesis is associated with blood-brain barrier permeability in temporal lobe epilepsy.* Brain, 2007. **130**(Pt 7): p. 1942-56.
39. Biron, K.E., et al., *Amyloid triggers extensive cerebral angiogenesis causing blood brain barrier permeability and hypervascularity in Alzheimer's disease.* PLoS One, 2011. **6**(8): p. e23789.
40. Chen, H.H., C.H. Chien, and H.M. Liu, *Correlation between angiogenesis and basic fibroblast growth factor expression in experimental brain infarct.* Stroke, 1994. **25**(8): p. 1651-7.
41. Yukawa, H., et al., *Adenoviral gene transfer of basic fibroblast growth factor promotes angiogenesis in rat brain.* Gene Ther, 2000. **7**(11): p. 942-9.
42. Luo, J., et al., *Hypoxia induces angiogenic factors in brain microvascular endothelial cells.* Microvasc Res, 2012. **83**(2): p. 138-45.
43. Mongiat, M., et al., *Extracellular Matrix, a Hard Player in Angiogenesis.* Int J Mol Sci, 2016. **17**(11).
44. Shiu, Y.T., et al., *The role of mechanical stresses in angiogenesis.* Crit Rev Biomed Eng, 2005. **33**(5): p. 431-510.
45. Rao, R.R., et al., *Matrix composition regulates three-dimensional network formation by endothelial cells and mesenchymal stem cells in collagen/fibrin materials.* Angiogenesis, 2012. **15**(2): p. 253-64.
46. Shamloo, A., et al., *A Comparative Study of Collagen Matrix Density Effect on Endothelial Sprout Formation Using Experimental and Computational Approaches.* Ann Biomed Eng, 2016. **44**(4): p. 929-41.
47. Feng, X., et al., *Fibrin and collagen differentially but synergistically regulate sprout angiogenesis of human dermal microvascular endothelial cells in 3-dimensional matrix.* Int J Cell Biol, 2013. **2013**: p. 231279.
48. Edgar, L.T., et al., *Extracellular matrix density regulates the rate of neovessel growth and branching in sprouting angiogenesis.* PLoS One, 2014. **9**(1): p. e85178.
49. Wang, J. and R. Milner, *Fibronectin promotes brain capillary endothelial cell survival and proliferation through alpha5beta1 and alphavbeta3 integrins via MAP kinase signalling.* J Neurochem, 2006. **96**(1): p. 148-59.

50. Zimmermann, D.R. and M.T. Dours-Zimmermann, *Extracellular matrix of the central nervous system: from neglect to challenge.* Histochemistry and Cell Biology, 2008. **130**(4): p. 635-653.
51. Yamaguchi, Y., *Lecticans: organizers of the brain extracellular matrix.* Cellular and Molecular Life Sciences, 2000. **57**(2): p. 276-289.
52. Sykova, E. and C. Nicholson, *Diffusion in brain extracellular space.* Physiological Reviews, 2008. **88**(4): p. 1277-1340.
53. Placone, A.L., et al., *Human astrocytes develop physiological morphology and remain quiescent in a novel 3D matrix.* Biomaterials, 2015. **42**: p. 134-43.
54. Partyka, P.P., et al., *Mechanical stress regulates transport in a compliant 3D model of the blood-brain barrier.* Biomaterials, 2017. **115**: p. 30-39.
55. Cho, H., et al., *Three-Dimensional Blood-Brain Barrier Model for in vitro Studies of Neurovascular Pathology.* Sci Rep, 2015. **5**: p. 15222.
56. Adriani, G., et al., *A 3D neurovascular microfluidic model consisting of neurons, astrocytes and cerebral endothelial cells as a blood-brain barrier.* Lab Chip, 2017. **17**(3): p. 448-459.
57. Herland, A., et al., *Distinct Contributions of Astrocytes and Pericytes to Neuroinflammation Identified in a 3D Human Blood-Brain Barrier on a Chip.* PLoS One, 2016. **11**(3): p. e0150360.
58. Wevers, N.R., et al., *A perfused human blood-brain barrier on-a-chip for high-throughput assessment of barrier function and antibody transport.* Fluids Barriers CNS, 2018. **15**(1): p. 23.
59. Uwamori, H., et al., *Integration of neurogenesis and angiogenesis models for constructing a neurovascular tissue.* Sci Rep, 2017. **7**(1): p. 17349.
60. Pun, P.B., J. Lu, and S. Moochhala, *Involvement of ROS in BBB dysfunction.* Free Radic Res, 2009. **43**(4): p. 348-64.
61. Kim, Y.W. and T.V. Byzova, *Oxidative stress in angiogenesis and vascular disease.* Blood, 2014. **123**(5): p. 625-31.
62. Stapor, P.C., et al., *Pericyte dynamics during angiogenesis: new insights from new identities.* J Vasc Res, 2014. **51**(3): p. 163-74.
63. Daneman, R., et al., *Pericytes are required for blood-brain barrier integrity during embryogenesis.* Nature, 2010. **468**(7323): p. 562-566.
64. Alvarez, J.I., et al., *The Hedgehog pathway promotes blood-brain barrier integrity and CNS immune quiescence.* Science, 2011. **334**(6063): p. 1727-31.
65. Gerhardt, H., et al., *Neuropilin-1 is required for endothelial tip cell guidance in the developing central nervous system.* Dev Dyn, 2004. **231**(3): p. 503-9.
66. Canfield, S.G., et al., *An isogenic neurovascular unit model comprised of human induced pluripotent stem cell-derived brain microvascular endothelial cells, pericytes, astrocytes, and neurons.* Fluids Barriers CNS, 2019. **16**(1): p. 25.
67. Jamieson, J.J., et al., *Role of iPSC-derived pericytes on barrier function of iPSC-derived brain microvascular endothelial cells in 2D and 3D.* Fluids Barriers CNS, 2019. **16**(1): p. 15.

68. Cudmore, R.H., S.E. Dougherty, and D.J. Linden, *Cerebral vascular structure in the motor cortex of adult mice is stable and is not altered by voluntary exercise (vol 37, pg 3725, 2017).* Journal of Cerebral Blood Flow and Metabolism, 2017. **37**(12): p. 3824-3824.
69. Whisler, J.A., M.B. Chen, and R.D. Kamm, *Control of perfusable microvascular network morphology using a multiculture microfluidic system.* Tissue Eng Part C Methods, 2014. **20**(7): p. 543-52.
70. Bezenah, J.R., Y.P. Kong, and A.J. Putnam, *Evaluating the potential of endothelial cells derived from human induced pluripotent stem cells to form microvascular networks in 3D cultures.* Sci Rep, 2018. **8**(1): p. 2671.
71. Linville, R.M., et al., *Modeling hyperosmotic blood-brain barrier opening within human tissue-engineered in vitro brain microvessels.* J Cereb Blood Flow Metab, 2019: p. 271678X19867980.

Figures

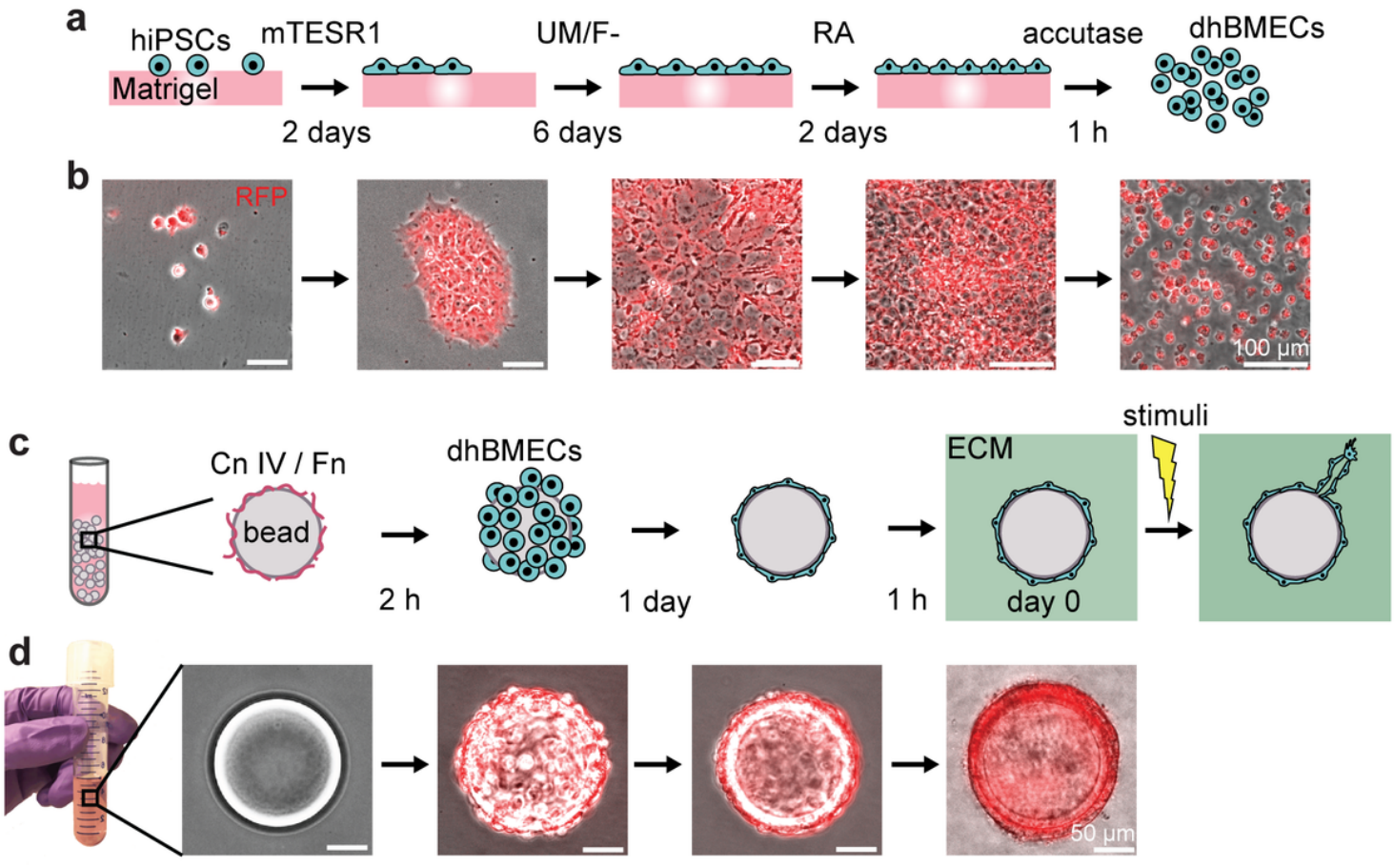

Figure 1

dhBMECs were differentiated from the WTC iPSC line with a fluorescently-tagged plasma membrane (Fig. 1a, b). 150 µm diameter beads were coated with extracellular matrix (ECM) proteins collagen IV and fibronectin, and then incubated with dhBMECs for 2 hours to achieve a uniform coating (Fig. 1c, d).

Figure 2

BBB beads display expression of critical BBB and endothelial markers, including claudin-5, occludin, glucose transporter 1 (GLUT1), p-glycoprotein (Pgp), and CD31 (Fig. 2a). Protein expression of BBB markers was unique to dhBMECs, while the endothelial marker (CD31) was also expressed by human umbilical vein endothelial cells (HUVECs) (Supp. Fig. 1). Additionally, BBB beads express the critical angiogenic ligand receptors fibroblast growth factor receptor 2 (FGFR2), vascular endothelial growth factor receptor 2 (VEGFR2), and G protein-coupled receptor 124 (GPR124) (Fig. 2b). BBB beads were incubated in Lucifer yellow (LY) for 3 hours to confirm formation of a functional barrier (Fig. 2c). Three conditions were tested: (1) blank beads without LY, (2) blank beads with LY, and (3) beads with dhBMEC monolayers with LY. The core of the beads is comprised of a permeable dextran polymer and hence beads without a dhBMEC monolayer showed high fluorescence intensity after three hours incubation with LY. In contrast, beads with a dhBMEC monolayer significantly restricted accumulation of solutes within the core ($p < 0.001$) (Fig. 2d-e). These results suggest that beads coated with dhBMECs display a key phenotypic property of the human BBB.

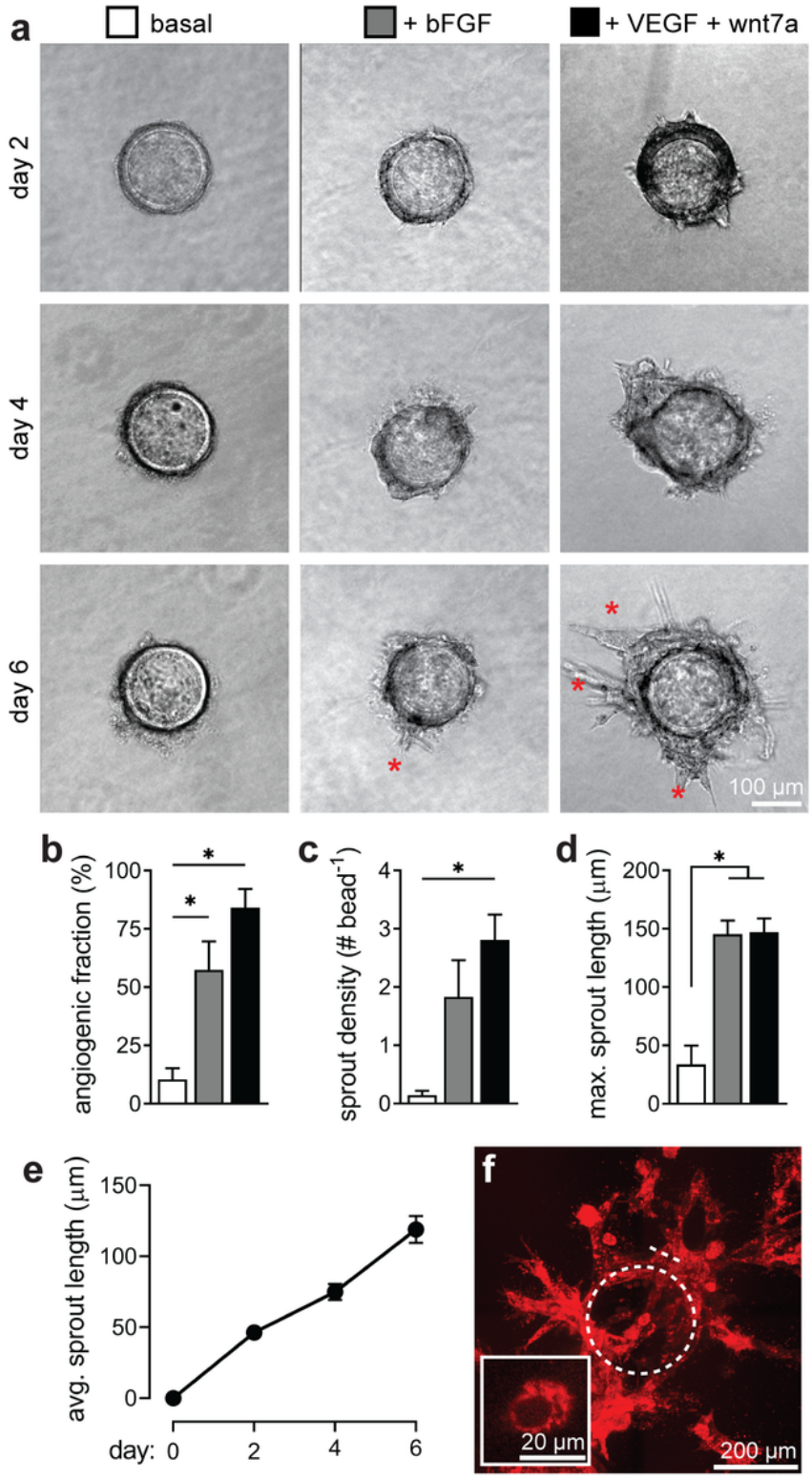

Figure 3

In the absence growth factors, angiogenic behavior was not widely observed (Fig. 3a): after six days, only 10% of beads displayed visible sprouts (Fig. 3b). In the presence of bFGF alone, some angiogenic behavior was observed. The angiogenic fraction and maximum sprout lengths were increased compared to beads cultured in the absence of bFGF ($p = 0.026$ and $p = 0.013$, respectively), while sprout density was not statistically different ($p = 0.097$) (Fig. 3b-d). The addition of VEGF and wnt7a produced on average

higher angiogenic phenotype (Fig. 3a), which was increased compared to basal conditions (p = 0.004, 0.012, and 0.018, respectively), but not statistically significant compared to bFGF exposure alone (Fig. 3b-d). The average sprout length for BBB beads in VEGF and wnt7a increased linearly with time with a growth rate of approximately 20 μm day-1 (Fig. 3e). Confocal imaging of BBB beads cultured in VEGF and wnt7a show extensive networks of angiogenic sprouts and formation of lumen-like structures (Fig. 3f).

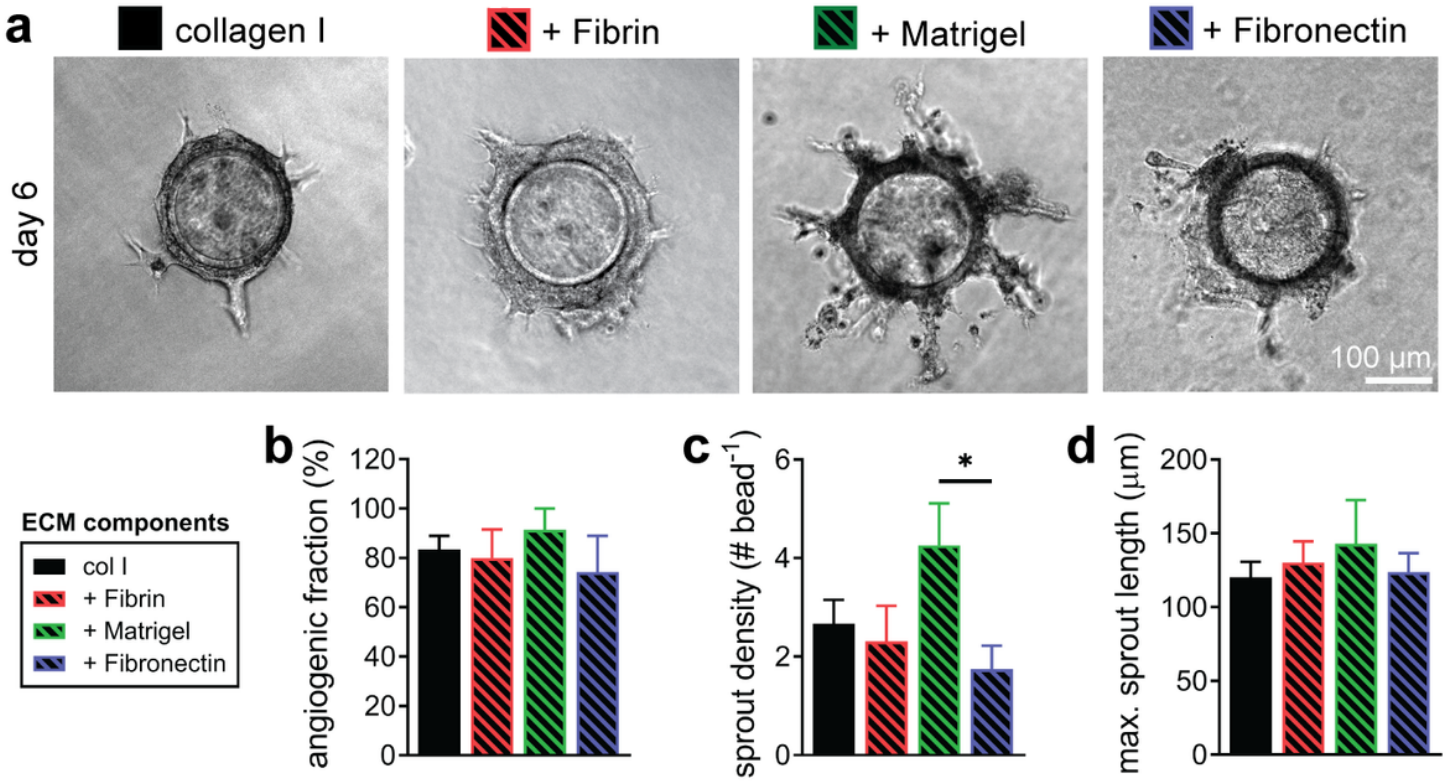

Figure 4

Changing ECM composition (without dramatically altering hydrogel biomechanics) had a less dramatic effect on angiogenic phenotype compared to soluble angiogenic factors: a similar sprouting morphology were observed across the conditions (Fig. 4a). The angiogenic fraction was similar across additions of ECM components and significant differences were not observed (p > 0.05 for all comparisons) (Fig. 4b). Matrigel supplementation led to increased sprout compared to fibronectin, suggesting that these two ECM conditions represent the most and least pro-angiogenic, respectively (p = 0.03) (Fig. 4c). Maximum sprout length was generally increased due to additions of ECM components, but was not significantly different (p > 0.05 for all comparisons) (Fig. 4d). For all subsequent experiments collagen I was supplemented with Matrigel to recapitulate angiogenic phenotype.

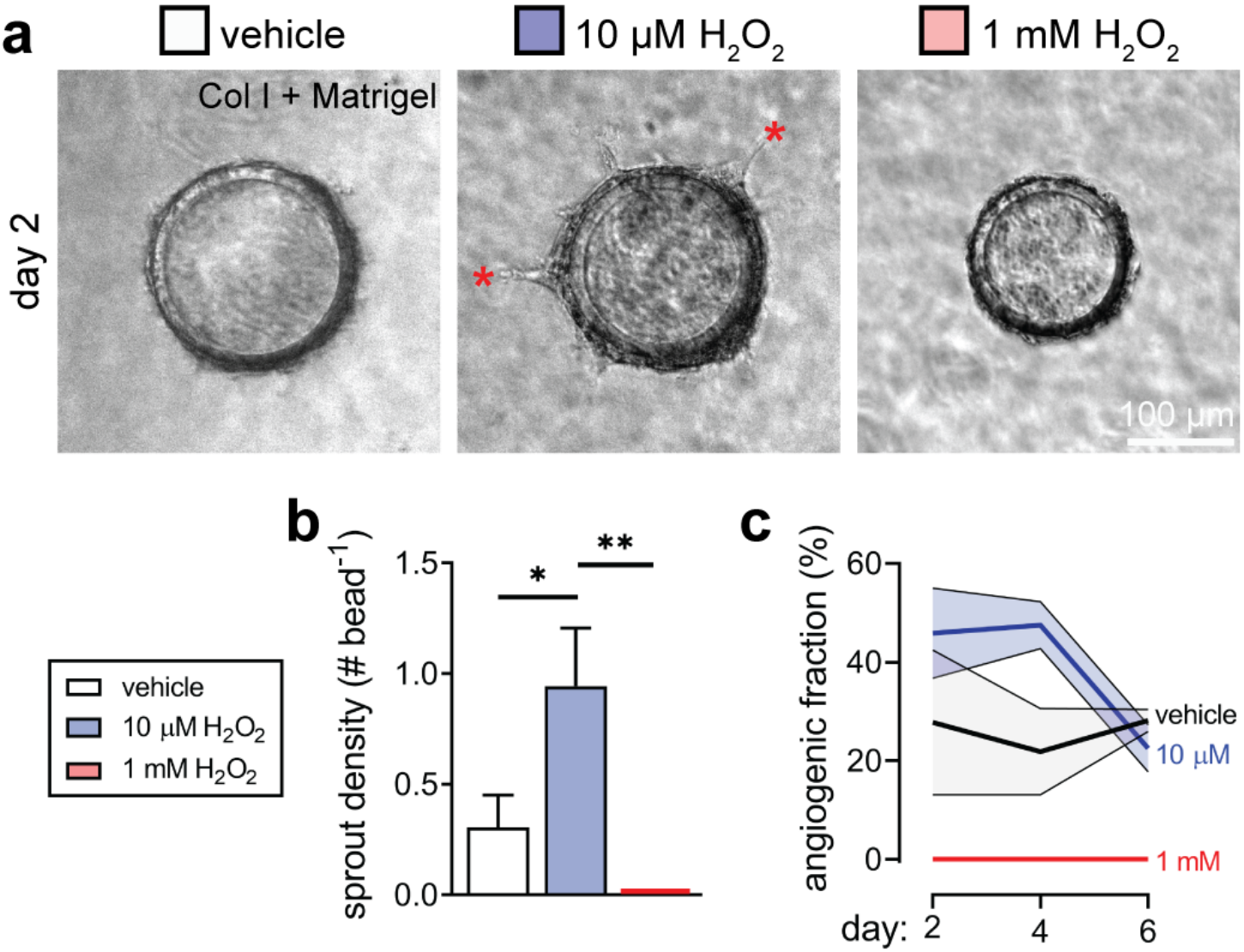

Figure 5

After two days exposure to 10 µM H2O2, the formation of sprouts into the ECM highlights an increased angiogenic phenotype (Fig. 5a). The sprout density was significantly increased compared to vehicle treatment ($p = 0.047$) (Fig. 5b). Interestingly, the pro-angiogenic effects of 10 µM H2O2 were not maintained over time as by day 6 angiogenic behavior was lost, while vehicle treatment displays minor angiogenic behavior (Fig. 5c). This suggests that 10 µM H2O2 exerts a bimodal effect of angiogenic phenotype. Interestingly, the addition of 100-fold higher H2O2 (1 mM) abrogates angiogenic behavior on much shorter time scales (no sprouts are observed) (Fig. 5a-c).

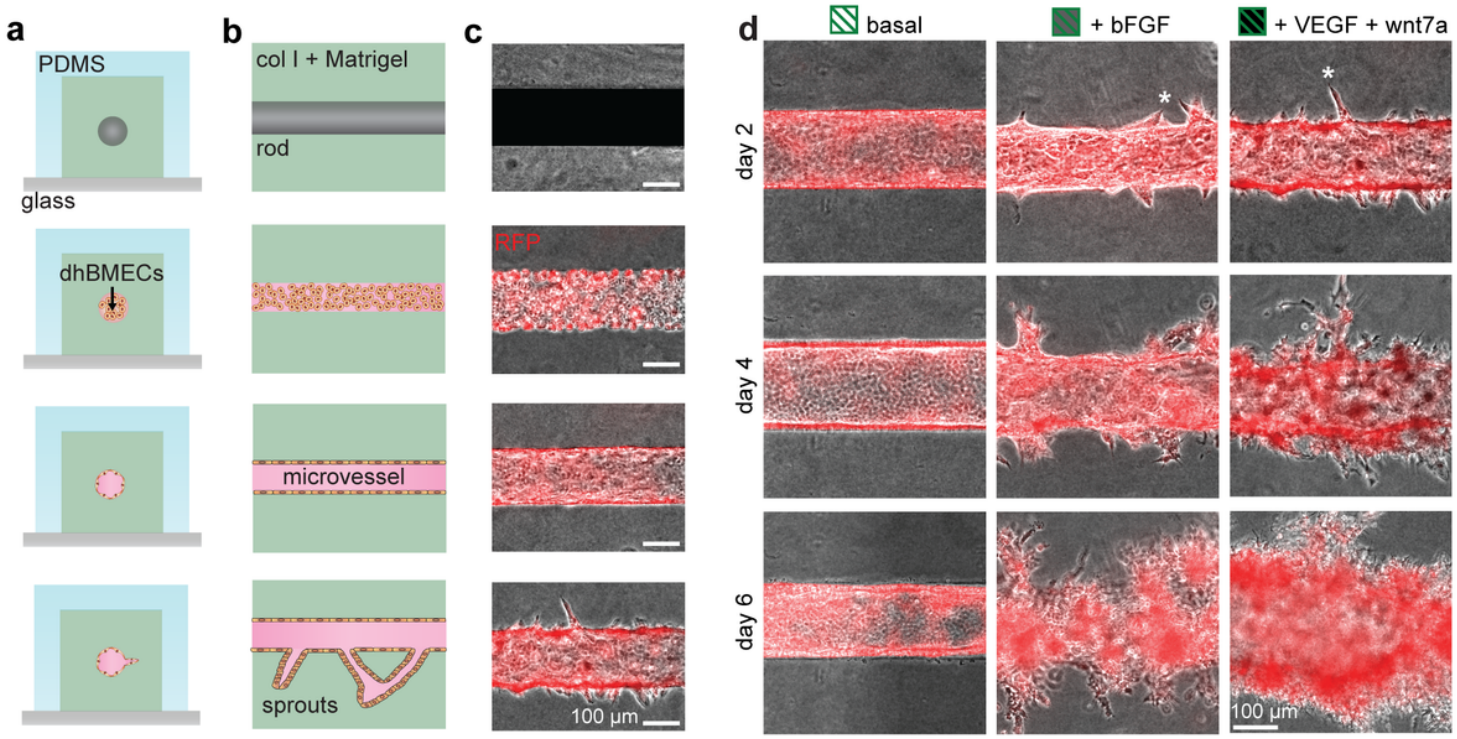

Figure 6

Microvessels are formed in 150 µm diameter channels within 6 mg mL-1 type I collagen supplemented with 1.5 mg mL-1 Matrigel (Fig. 6a, b). Channels are seeded with dhBMECs, which under continual ~2 dyne cm-2 perfusion, assemble into BBB microvessels as previously reported [27]. After microvessel formation, we applied media conditions as tested in Figure 3 to observe angiogenic behavior (Fig. 6c). Under perfusion with basal media, angiogenic behavior is not widely observed and the microvessel structure remains stable over six days (Fig. 6d). Supplementation with bFGF results in early sprouts within two days, which continue to grow in length and branching complexity (Fig. 6d). Supplementation with bFGF, VEGF, and wnt7a resulted in an increased density of sprouts along microvessels after two days, and chaotic sprouting behavior by six days (Fig. 6d)

Figure 7

We patterned adjacent 150 µm diameter channels within 6 mg mL-1 type I collagen supplemented with 1.5 mg mL-1 Matrigel separated by 200 µm (Fig. 7a, b). After microvessel formation, microvessels were perfused at ~2 dyne cm-2 with basal media + 20 ng mL-1 bFGF (Fig. 7c). Continual perfusion over three days resulted in anastomosis of capillary sprouts (Fig. 7d).